Received: 3 May 2019 | Revised: 5 July 2019 | Accepted: 10 July 2019
DOI: 10.1002/ldr.3411

RESEARCH ARTICLE

# Wildfire severity: Environmental effects revealed by soil magnetic properties

Neli Jordanova[1] | Diana Jordanova[1] | Vidal Barrón[2]

[1] National Institute of Geophysics, Geodesy and Geography, Bulgarian Academy of Sciences, Acad. G. Bonchev, block 3, 1113 Sofia, Bulgaria

[2] Department of Agronomy, University of Córdoba, Edificio C4, Campus de Rabanales, 14071 Córdoba, Spain

**Correspondence**
Neli Jordanova, National Institute of Geophysics, Geodesy and Geography, Bulgarian Academy of Sciences, Acad. G. Bonchev, block 3; 1113 Sofia, Bulgaria.
Email: neli_jordanova@hotmail.com

**Funding information**
Bulgarian National Science Fund, Grant/Award Numbers: DFNI K02-13, DFNI K02/13; INTERREG-POCTEP: "Centro Ibérico para la Investigación y Lucha contra Incendios Forestales", Grant/Award Number: 0753_CILIFO_5_E

## Abstract

Strong wildfires pose significant damage to all soil qualities and lead to land degradation. The complex nature and properties of fire-derived materials require multidisciplinary efforts for their reliable characterization. The main objective of our study was to evaluate the suitability of magnetic properties of fire-affected soils as proxy parameters for wildfire severity and to relate magnetic signature of burnt soils to carbon and nitrogen contents as influenced by wildfires. We present mineral magnetic investigation of 22 sites with wildfire-affected soils and 17 nonburnt soils from nearby locations. We employed measurements of magnetic susceptibility and anhysteretic remanence in combination with scanning and transmission electron microscopy observations on magnetic particles from burnt soils and ashes. Bulk soil and vegetation ash analyses of total carbon and nitrogen, organic carbon, and elemental content were carried out as well. We show that pyrogenic magnetic enhancement is restricted to the uppermost 0- to 2-cm soil depth and can be used as a proxy for wildfire severity. Strong wildfires lead to the production of nanometer-sized superparamagnetic magnetite and/or maghemite particles and smaller amount of single-domain fraction. These strongly magnetic minerals have typical characteristics of high-temperature combustion products with spherical shape and diameters between 0.1 and 2 μm. Fire-affected soils show relative enrichment with phosphorous, manganese, and heavy metals (Cu, Pb, Zn, Ni, Co, and As) calculated with respect to soils from nonburnt nearby localities. Our results demonstrate the potential of environmental magnetic methods as an additional tool for assessment of wildfire severity and the content of main soil nutrients.

**KEYWORDS**

fire severity, magnetic susceptibility, pyrogenic magnetic enhancement, soil, total carbon, wildfire

## 1 | INTRODUCTION

Wildland fires are among the major factors controlling ecosystem functioning, and their effects on the soil compartment are crucial for the sustainable land use and management. Moreover, fire-induced disturbance of the ecosystems leads to changes in carbon sequestration, soil fertility, erosion, and biodiversity (Bento-Gonçalves, Vieira, Úbeda, & Martín, 2012; Mataix-Solera, Cerdá, Arcenegui, Jordán, & Zavala, 2011). In this respect, wildfires can provoke land degradation, and their effects need to be carefully evaluated for taking proficient measures for soil restoration and development. Therefore, fire is regarded as a soil-forming factor (Certini, 2014; Santín & Doerr, 2016). The largest carbon pool on the Earth is in soil, and the organic carbon makes up about 70% of it, whereas the remaining amount is fixed in carbonates (González-Pérez, González-Vila, Almendros, & Knicker, 2004). During wildfires, gaseous products ($CO_2$, $CH_4$, and $H_2O$) are emitted into the atmosphere, and solid residues in the form of particulate organic matter in the ash and char from incompletely burned vegetation are added to the soil. Therefore, the carbon pool in the soil is expanded by the 'pyrogenic' carbon formed during fires. Carbon dioxide emitted in the atmosphere is taken up by the new vegetation through photosynthesis and enters again the soil carbon turnover. Heat generated during wildfires influences directly soil microbial biomass by modifying the balance between various bacterial and fungal communities (Knicker, 2007; Mataix-Solera, Guerrero, García-Orenes, Bárcenas, & Torres, 2009). At the same time, ash produced during fires contains considerable stock of water-soluble microelements that play a role of fertilizer for the subsequent soil and vegetation recovery (González-Pérez et al., 2004; Mataix-Solera et al., 2009). Within this complex system of interactions among different physical, geochemical, and biological factors, iron oxides play an important role with their strong sensitivity to changing redox conditions, solute chemistry, temperature, and microbial activities (Cornell & Schwertmann, 2003; Melton, Swanner, Behrens, Schmidt, & Kappler, 2014).

Iron oxyhydroxides as ferrihydrite ($Fe_{10}O_{14}(OH)_2 \cdot nH_2O$), goethite (α-FeOOH), lepidocrocite (γ-FeOOH)), and hematite (α-$Fe_2O_3$) are the major forms of iron in soils as products of weathering reactions of the soil parent rock material (Barrón & Torrent, 2013; Schwertmann, 1988). Strongly magnetic iron oxides in soils are magnetite ($Fe_3O_4$), which is generally lithogenic, and in many cases a precursor of pedogenic maghemite (γ-$Fe_2O_3$). Both minerals are not easy to distinguish because different intermediates with gradual iron oxidation can be present and furthermore occur as minor constituent (around 0.1 up to 2 wt%) in most of the soils from temperate climate area. The amount and grain size distribution of this pedogenic strongly magnetic fraction is a sensitive proxy for the mean annual precipitation (MAP) in well-aerated soils developed on loess (Maher, 1986; Maher, 2016). Pedogenic maghemite is also considered to originate and transform during the geological time scale by ferrrihydrate transformations (Jiang et al., 2018). Specific peculiarity of the magnetic signature of fire-affected soils is their strong magnetic enhancement, restricted to the uppermost 0- to 2-cm depth (Jordanova, Jordanova, Barrón, & Petrov, 2018; Le Borgne, 1955; Rummery, Bloemendal, Dearing, & Oldfield, 1979). The origin of the increased production of magnetite (and then maghemite, as a product of the pedogenic oxidation from the magnetite precursor) as a result of fire is still disputable. Besides thermally induced transformations of the mineral soil (Carrancho & Villalaín, 2011; Kletetschka & Banerjee, 1995; Le Borgne, 1955; Oldfield & Crowther, 2007), other mechanisms have been recently proposed, namely, formation of strongly magnetic Fe oxides in vegetation ash and their deposition on soil surface (Jordanova et al., 2018) and microbially mediated formation of strongly magnetic iron oxides shortly after a (wild)fire event (Jordanova, Jordanova, Mokreva, Ishlyamski, & Georgieva, 2019).

The main objective of our study was therefore to evaluate the potential of mineral magnetic parameters of burned soils to serve as an alternative independent proxy for assessment of wildfire severity and content of main nutrients in wildfire-affected areas. In order to achieve this goal, we carried out detailed magnetic investigations of burnt soils and their nonburnt counterparts for establishment of iron oxide mineralogy and magnetic grain size of natural and fire-produced magnetic particles. In combination with chemical analyses, microscopy observations, and X-ray diffraction, we analyzed different relationships among magnetic and nonmagnetic characteristics of burned soils. We reveal the effect of fire severity on the amount of the pyrogenic magnetic enhancement of soils and its utilization as a suitable indicator for changes in carbon and nitrogen storage in fire-affected soils.

## 2 | MATERIALS AND METHODS

### 2.1 | Locations and sampling

Forest wildfires are a common phenomenon for the territory of Bulgaria during the summer season, and the frequency of wildfire events increases progressively during the last decades (Panayotov et al., 2017). Each year, about 5% of the forests in Bulgaria are affected by wildfires and put in danger wide areas protected by the NATURE2000 regulation.

Twenty-two locations of wildfire-affected soils and 17 sites of natural soils close to each burnt area have been studied. Specific locations were identified on the basis of information available for fire occurrence (site, date, and severity), type of vegetation (pine, broadleaf or mixed forests, grasslands, shrubs, etc.), and the time since a fire event. The oldest wildfire event among the sampled locations occurred in year 2000, and the most recent, in summer 2017 (1 week before sampling). One site of experimental fire (Jordanova et al., 2019) was also included in the study as a reference for zero-time-since fire. All fire-affected sites recovered naturally after the fire without targeted post-fire reforestation measures. Detailed description of wildfire-affected sites and natural soils (indicated by an index 'n') is presented in Table 1, and some examples of the landscapes are shown in Figure S1. Fire severity class (Table 1 and further in data interpretation) was ascribed on the basis of field observations in case of recent fires, and for past fires - on the basis of fire department archives, press publications, and reports available. We use the classification proposed by Keeley (2009) and introduce the following nomenclature: strong fire severity—marked by the symbol '1'; moderate severity, '2'; and light (weak) severity, '3.'

Having in mind the general high nonhomogeneity of the fire severity on a local scale (Bento-Gonçalves et al., 2012; Bodí et al., 2014), we have chosen profile sampling locations within the burnt areas at spots showing signs of the strongest impact on soil, for example, thick ash layer, maximum consumed vegetation cover, minor pieces of evidence for postfire soil erosion.

At each site, soil profile was dug, described, and sampled at high-resolution continuous sampling—at 0.5-cm interval for the uppermost 5 cm, at 1-cm interval at depths 5–10 cm, and at 2 cm interval downward to 20-cm (30-cm) depth. Sampling to a depth well below the fire influence aimed to reveal changes in iron oxide content and mineralogy in various soil horizons (Goforth, Graham, Hubbert, Zanner, &

**TABLE 1** Description of study sites

| Site | Abbreviation | Soil type | Vegetation | Elevation (m a.s.l.) | Wildfire event | Fire severity | Aspect | Soil pH | Geology | Latitude (N) | Longitude (E) |
|---|---|---|---|---|---|---|---|---|---|---|---|
| STUDENA | ST | Cutanic Luvisol | Pine | 440 | 2013 | 1 | E | 6 | Granite | 41°53′18.30″ | 6°21′53.70″ |
| | STn | Cutanic Luvisol | Pine | 424 | | | E | 5.8 | Granite | 41°53′23.80″ | 6°21′26.20″ |
| STARA KRESNA | STK | Chromic Luvisol | Pine | 619 | 2017 | 1 | SW | 5.9 | Sandstone | 41°47′32.40″ | 3°11′47.80″ |
| | STKn | Chromic Luvisol | Pine | 695 | | | SW | 5.5 | Sandstone | 41°47′46.80″ | 3°13′16.60″ |
| MALJOVITZA | M | Umbrisol | Pine | 1,977 | 2000 | 1 | N | 4.2 | Granite | 42°11′53.40″ | 23°22′52.50″ |
| | MO | Umbrisol | Pine | 1,733 | | | N | 4.6 | Granite | 42°12′49.0″ | 23°23′15.30″ |
| PANCHEVO | PAN | Cutanic Luvisol | Pine | 355 | 2000 | 1 | Summit | 6.0 | Volcanic rocks, zeolites | 41°38′47.90″ | 5°24′58.40″ |
| BRJAKOVTZI | BRI | Cutanic Luvisol | Pine | 987 | 2012 | 2 | W | 7.2 | Limestones, dolomites | 43°3′49.40″ | 23°9′10.50″ |
| | BRIn | Cutanic Luvisol | Pine | 980 | | | W | 7.5 | Limestones, dolomites | 43°3′49.30″ | 23°9′07.90″ |
| SLIVEN | SLV | Cutanic Luvisol | Pine | 607 | 2012 | 1 | SE | 5.8 | Limestones, dolomites | 42°42′54.60″ | 6°20′32.00″ |
| | SLVn | Cutanic Luvisol | Pine | 620 | | | SE | 5.1 | Limestones, dolomites | 42°42′54.50″ | 6°20′29.30″ |
| HISARJA | HSR | Cutanic Luvisol | Pine | 270 | 2013 | 1 | Flat | 6.3 | Weathered granite | 42°28′12.40″ | 4°44′56.50″ |
| | HSRn | Cutanic Luvisol | Pine | 264 | | | Flat | 5.6 | Weathered granite | 42°28′14.60″ | 4°44′54.80″ |
| VITOSHA-ALEKO | VIT | Cambisol | Pine | 1,753 | 2012 | 2 | E | 5.8 | Granite | 42°34′27.80″ | 3°17′52.80″ |
| | VITn | Cambisol | Pine | 1,763 | | | E | 4.8 | Granite | 42°34′07.30″ | 3°17′55.60″ |
| BINKOS | BK | Cutanic Luvisol | Pine | 259 | 2015 | 2 | NW | 6 | Sandstones, argillites | 42°38′54.60″ | 26°7′21.00″ |
| | BKn | Cutanic Luvisol | Pine | 263 | | | NW | 6.5 | Sandstones, argillites | 42°38′55.00″ | 26°7′21.90″ |
| GRADINA | GRD | sand | Pine | 30 | 2016 | 3 | Flat | | Sands | 42°24′26.30″ | 27°39′44.7″ |
| | GRDn | sand | Pine | 30 | | | Flat | | Sands | 42°24′26.30″ | 27°39′44.7″ |
| EXPERIM. FIRE | EF | Cambisol | Pine | 924 | 2015 | 2 | SE | 6.7 | Conglomerates, sandstones | 42°27′27.70″ | 23°30′41.00″ |
| SLIVOVO | SL | Cutanic Luvisol | Oak | 321 | 2012 | 2 | N | 6.6 | Metamorphic rocks | 42°12′34.90″ | 27°0′50.70″ |
| RAJNOVO | R | Mollic Vertisol | Oak | 70 | 2013 | 2 | S | 7.6 | Clays, sandstones | 42°0′44.80″ | 5°46′07.90″ |
| | Rn | Mollic Vertisol | Oak | 98 | | | S | 6.9 | Clays, sandstones | 42°01′05.90″ | 5°45′06.20″ |
| VLAHI | VL | Chromic Luvisol | Hornbeam/grass | 619 | 2017 | 2 | SE | 7.9 | Conglomerates | 41°44′47.70″ | 3°13′57.10″ |
| | VLn | Chromic Luvisol | Hornbeam/grass | 619 | | | SE | 7.0 | Conglomerates | 41°44′47.60″ | 3°13′57.00″ |
| BRIAST | BR | Mollic Vertisol | Hornbeam/grass | 72 | 2015 | 3 | Flat | 7.3 | Clays, sandstones | 42°6′57.20″ | 5°37′14.10″ |
| | BRn | Mollic Vertisol | Hornbeam/grass | 75 | | | Flat | 6.8 | Clays, sandstones | 42°6′57.20″ | 5°37′17.70″ |
| KLIMENT | KL | Cutanic Luvisol | Mixed | 256 | 2013 | 1 | Flat | 6 | Metamorphic rocks, gneiss | 42°35′8.90″ | 24°43′17.20″ |
| | KLn | Cutanic Luvisol | Mixed | 253 | | | Flat | 5.6 | Metamorphic rocks, gneiss | 42°35′6.60″ | 4°43′28.40″ |
| PASTRA | PAS | Cutanic Luvisol | Mixed | 944 | 2012 | 2 | W | 6.3 | Metamorphic rocks, gneiss | 42°7′37.90″ | 23°14′34.80″ |
| OKOL | GO | Cambisol | Mixed | 1,048 | 2008 | 2 | SE | | Conglomerates | 42°27′33.50″ | 23°30′11.30″ |
| | GOn | Cambisol | Mixed | 924 | | | SE | 4.5 | Conglomerates | 42°27′35.30″ | 3°30′40.10″ |
| RAZGRAD | RZ | Luvic Phaeozem | Grass + bushes | 250 | 2015 | 2 | Flat | 7.7 | Loess | 43°30′53.19″ | 6°32′48.48″ |
| | RZn | Luvic Phaeozem | Grass + bushes | 250 | | | | 7.5 | Loess | 43°30′53.19″ | 6°32′48.48″ |
| PLEVEN | PLV | Leached Chernozem | Grass | 262 | 2015 | 3 | Flat | | Loess | 43°25′32.22″ | 4°41′43.19″ |

(Continues)

**TABLE 1** (Continued)

| Site | Abbreviation | Soil type | Vegetation | Elevation (m a.s.l.) | Wildfire event | Fire severity | Aspect | Soil pH | Geology | Latitude (N) | Longitude (E) |
|---|---|---|---|---|---|---|---|---|---|---|---|
| | PLVn | Leached Chernozem | Grass | 262 | | | Flat | 8.0 | Loess | 43°25′32.22″ | 4°41′43.19″ |
| KOSHAVA | KO | Calcic Chernozem | Grass | 32 | 2011 | 3 | Flat | 7.9 | Loess | 44°05′01.40″ | 3°01′24.40″ |
| | KOn | Calcic Chernozem | Grass | 32 | | | Flat | 7.6 | Loess | 44°05′01.40″ | 3°01′24.40″ |
| YAMBOL | Y | Chromic Luvisol | Grass | 180 | 2017 | 3 | Flat | 5.7 | Volcanic rocks, tuffites | 42°29′12.30″ | 26°32′33.10″ |
| | Yn | Chromic Luvisol | Grass | 180 | | | Flat | 7.2 | Volcanic rocks, tuffites | 42°29′12.30″ | 26°32′33.10″ |

*Note*. In the abbreviation of a site's name, the suffix "n" denotes natural soils. Soil classification in column 3 is according to World Reference Base. Soil reaction (pH) in column 9 refers to the uppermost 1 cm from the soil depth.

Minnich, 2005; Oldfield & Crowther, 2007). Because natural soils were sampled as close as possible to the fire-affected sites, they can be regarded as their independent replicates for the nonburnt depth levels. Fire-affected levels show wide variability in magnetic properties, corresponding to high nonhomogeneity in fire intensity across even a restricted area (Bento-Gonçalves et al., 2012; Bodí et al., 2014; Goforth et al., 2005). Representative examples of typical fire-affected soil profiles are shown in Appendix A.

Bulk powder material of about 100-g weight was gathered from each depth interval, packed in zip seal plastic bags and transported to the laboratory. After air-drying, the material was sieved through 1-mm sieve and used for further analyses. Vegetation ashes and charred wood were separately gathered from several locations of recent wildfires for verifying the input of vegetation cover to the total elemental composition and magnetic signal of burnt soils.

## 2.2 | EXPERIMENTAL METHODS

### 2.2.1 | Magnetic measurements

Magnetic susceptibility is a basic mineral magnetic parameter widely utilized for deducing the concentration of strongly magnetic iron oxides in soils (Evans & Heller, 2003; Walden, Oldfield, & Smith, 1999). Magnetic susceptibility measurements were done on bulk powder material, filled in standard 10-cm$^3$ plastic cylinders using magnetic susceptibility Kappabridge MFK 1A (AGICO, Czech Republic) with a sensitivity of $2 \times 10^{-8}$ International System of Units (SI), an applied field of 300 A/m, and a working frequency of 976 Hz. Mass-specific susceptibility (χ) was calculated by dividing volume magnetic susceptibility, obtained with the Kappabridge by the sample weight, measured on an analytical balance KERN ABJ with a precision of 0.0001 g.

Anhysteretic remanent magnetization (ARM) is a laboratory-induced magnetization that is used in environmental magnetic studies to infer the content of fine-grained single-domain magnetite/maghemite particles in different natural materials, including soil (Evans & Heller, 2003; King, Banerjee, Marvin, & Ozdemir, 1982; Maher, 1988; Walden et al., 1999). ARM was imparted using a Molspin alternating field tumbling demagnetizer with a 100-mT maximum amplitude of the alternating field and the ARM attachment with an applied weak direct current field of 0.1 mT (Molspin Ltd., UK).

Magnetic characterization and phase identification of the remanence carriers were accomplished using stepwise thermal demagnetization of composite isothermal remanent magnetization (IRM), acquired along the three perpendicular sample's axes (Lowrie, 1990), and IRM stepwise acquisition curves, analyzed using distribution of cumulative Gaussian functions (Robertson & France, 1994; Stockhausen, 1998). Each magnetic component is characterized by its saturation IRM, the field at which half of the saturation IRM is reached ($B_{1/2}$), and the width of the distribution, expressed through the dispersion parameter Dispersion Parameter (DP) (one standard deviation of the logarithmic distribution) (Kruiver et al., 2001). IRM unmixing was done using the MAXUnMix software (Maxbauer et al., 2016a). IRM was acquired using an IM-10-30 impulse magnetizer with a maximum field of 5 T (ASC Scientific, USA). In a thermal demagnetization experiment (Lowrie, 1990), a high-coercivity fraction (hard component) was delineated along the *z*-axis by applying a direct current field of 5 T. A medium-coercivity component was separated along the *y*-axis by applying a field of 600 mT, and a low-coercivity (soft) magnetic fraction was magnetized along the *x*-axis using a field of 200 mT. Thermal demagnetization of components, characterized by known coercivity, provides more diagnostic information on magnetic minerals' identification (Walden et al., 1999). Remanence measurements were carried out using a JR 6A spinner magnetometer (AGICO, Czech Republic) with a sensitivity of $2.4 \times 10^{-6}$ A/m.

### 2.2.2 | Nonmagnetic analyses

Soil pH was measured with a Hanna 213 pH meter (Hanna Instruments, USA) in water (1:5 soil–water ratio with a sample holding time of 1 hr).

Qualitative X-ray diffraction analysis was performed on 12 bulk powder samples using a Bruker D8 ADVANCE X-ray diffractometer with monochromatic Cu Kα radiation.

Elemental composition of 48 selected samples from different depths of fire-affected soil profiles as well as from the topmost levels of natural soils was determined after Aqua regia extraction (reference method US_EPA 3051a). The analysis consists of digestion of 1.5 g of soil diluted in 10.5 ml of 35% HCl and 3.5 ml of 65% $HNO_3$, heating at 180 °C for 20 min in a microwave system (Anton Paar Multiwave 3000). Aliquots of 50 ml were analyzed with an inductively coupled plasma atomic emission spectroscopy dual view (Thermo ICap 6500).

Additional data on the composition of nine vegetation ashes and wood charcoal samples were obtained by X-ray fluorescence (XRF) analysis using the portable XRF instrument S1 TITAN Model 800 (Bruker Elemental, USA) and calibration standard—soil sample CS-M2GEO. The material was finely grounded and pressed before measurements. Readings were taken at three different points per sample, and mean value was calculated for each sample and element measured.

Observations on single particles using the scanning electron microscope JEOL JSM6390 coupled with an energy-dispersive X-ray (EDX) INCA Oxford analyzer were performed after carbon or gold coating the surface.

The high-resolution transmission electron microscope JEOL JEM 2100 (JEOL Ltd., Japan) was utilized for examination of selected samples using an accelerating voltage of 200 kV. The samples were sonicated, and suspensions were dropped on standard Cu grids coated with amorphous carbon. Observations were carried out after sample drying in a clean atmosphere under ambient conditions.

Determination of total N and C was accomplished for 50 samples by the calcination method using an LECO CN analyzer, and the organic C was determined through oxidation by $K_2Cr_2O_7$ (Walkley–Black) on two replicates. The ‘pyrogenic change’ in the content of $C_{tot}$, $C_{org}$, $N_{tot}$, and so on, was calculated as the content of C (or N) in the topsoil sample, most affected by fire, divided by the corresponding content in a sample from the same depth from the natural profile. Here we have considered as more appropriate for normalization purposes the corresponding concentrations of nutrients in the topsoil samples from the paired natural nonburnt soil profiles instead of the deeper levels of the burnt soils because of much stronger concentration gradients in nutrients content along soil depth. The obtained ratios are indicative of wildfire-induced changes but keeping the influence of the soil type and its intrinsic pedogenic properties. To test the statistical significance of the difference between pairs of groups obtained from the relation between pyrogenic magnetic enhancement and the fire severity, Tukey honestly significant difference post hoc test with unequal number (*N*) observations have been carried out using the STATISTICA 7.0 software.

## 3 | RESULTS

### 3.1 | Variations of magnetic susceptibility and anhysteretic remanece along the depth of soil profiles

Variations of mineral magnetic parameters with depth of fire-affected and natural soils. The variations of magnetic properties along depth of the fire-affected soil profiles show a typical pattern of strong enhancement in the uppermost centimeters of all concentration-dependent magnetic parameters. The best expression of this phenomenon is the behavior of mass-specific magnetic susceptibility (χ) and anhysteretic remanence (ARM), because of the dominant contribution of the fine-grained (nanometer-sized) superparamagnetic (SP) and single-domain magnetite (maghemite) to the total signal (Maher, 1988). Examples of typical depth variations of χ and ARM for pairs of burnt and nonburnt soil profiles included in the present study are given in Figure 1. For the rest of the profiles studied, analogous graphs are shown in Figure S2. It is obvious that magnetic data for fire-affected soil profiles show much higher χ and ARM values in the uppermost 0- to 2-cm depth (Figure 1) as compared with respective depths from the nonburnt replica soil. Except for few particular cases (the high-mountain soil profile M and the profile BR; Figure S2), the strongest fire-induced magnetic enhancement is observed in the topmost surface levels (the uppermost 1–2 cm). These values are regarded as representing the maximum fire-induced changes in the soil magnetic mineralogy. In order to extract this signature from the original (natural) soil magnetic enhancement, resulting from the pedogenic *in situ* formation of submicrometer magnetite fraction (Jordanova, 2016; Maher, 1986), we define a maximum of ‘pyrogenic magnetic enhancement’ as

$$\chi_{\text{pyrogenic}} = \chi_{\text{fire-affected}} / \chi_{\text{natural}},$$

$$\text{ARM}_{\text{pyrogenic}} = \text{ARM}_{\text{fire-affected}} / \text{ARM}_{\text{natural}},$$

where the values of $\chi_{\text{fire-affected}}$ and $\text{ARM}_{\text{fire-affected}}$ are taken for the depth of maximum enhancement. The values of χ and ARM of natural nonburnt material were considered those from the deeper level (in most cases at depth of 5 cm) of the burnt profile itself because between-sites spatial variation in the magnetic signal could be larger. Thus, the total pyrogenic magnetic enhancement is calculated as the sum of the two components ($\chi_{\text{pyrogenic}}$ + $\text{ARM}_{\text{pyrogenic}}$).

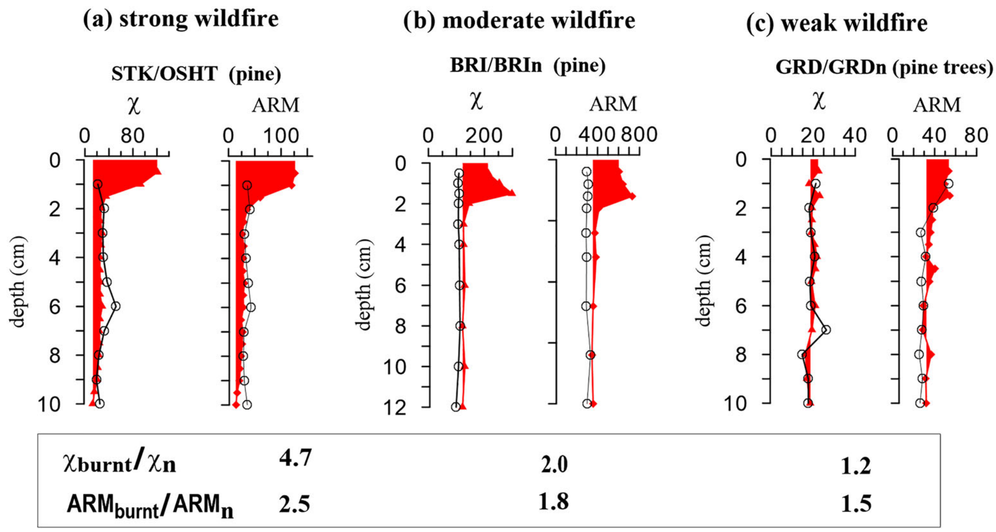


**FIGURE 1** Depth variations of magnetic susceptibility (χ, in $10^{-8}$ $m^3$/kg) and anhysteretic remanent magnetization (ARM, in $10^{-6}$ A·$m^2$/kg) along burnt (full red symbols and red shaded area) and natural (open circles) soil profiles for the sampled locations. Enhancement ratios of χ and ARM, calculated as the maximum value for burnt profile to the nonburnt counterpart are also shown below each example [Colour figure can be viewed at wileyonlinelibrary.com]

As it is seen in Figure 1, magnetic enhancement expressed by χ and ARM is strongest at the site burnt by a strong fire (Figure 1a), is less intense in the site affected by moderate wildfire (Figure 1b), and is not unambiguously clear in case of a weak wildfire (Figure 1c). Similar observations can be seen for the rest of the sites studied (Figure S2). In general, grass fires and weak wildfires in broadleaf forests display more subtle changes in magnetic characteristics of the topsoil levels, whereas in conifer forests the effect of fire is explicitly expressed as a sharp peak in χ and ARM.

## 3.2 | Magnetic mineralogy

Magnetic minerals identification in soils is important because different iron oxides possess different magnetic properties that can influence the overall expression of their magnetic signal. Magnetic minerals, carrying the signature of the fire-affected soil levels and natural samples, have been identified using thermal demagnetization of composite IRM through the observed unblocking temperatures of the three coercivity components (Lowrie, 1990) and unmixing of IRM acquisition curves (Kruiver et al., 2001; Maxbauer et al., 2016a). Representative examples of results from these diagnostic experiments are shown in the Supporting Information (Figures S3 and S4). There is no systematic difference between the obtained unblocking temperatures for samples originating from burnt versus nonburnt levels. Major contribution to the total remanence comes from the low-coercivity component, which unblocks at temperatures in the range of 570–620 °C. Some differences in the shape of the demagnetization curves of the soft components are revealed, depending on the site. Comparison between demagnetization curves for burnt and nonburnt soil samples shows that the main component affected by fire is the soft one. It shows generally one order of magnitude stronger intensity, as compared with the soft component in nonburnt soils (Figure S3). In contrast, the medium and hard components display similar shapes and intensities in all pairs of samples. The medium component unblocks at temperatures similar to the unblocking of the soft component, whereas the hard component unblocks usually at ~700 °C or has almost no contribution to IRM (Figure S3).

IRM acquisition curves were obtained for three samples from burnt by strong-wildfire sites (HSR, STK and PAN) and two nonburnt levels from one site (HSR). The obtained results from coercivity components extraction by unmixing IRM curves (Kruiver et al., 2001; Maxbauer et al., 2016a) are shown in Figure S4 together with numerical values obtained for the characteristics of the components. The analysis confirms the dominating contribution of magnetically soft minerals in all samples (Figure S4). Detailed investigation of the coercivity parameters of the extracted components shows that the coercivity ($B_{1/2}$) of the soft component in burnt soils is close to 40 mT in all three samples analyzed, whereas in nonburnt soil it is slightly lower (~35 mT). The hard component is identified in all samples and has high coercivities, generally above 1,000 mT.

## 3.3 | Microscopy observations

Surface morphology of the Fe-containing particles, responsible for the enhanced magnetic signal of fire-affected soil levels, was observed through scanning electron microscopy. Iron-containing particles identified display typical spherical shapes, indicating high-temperature origin (Figure S5). Typical Fe-rich spherules with dense homogeneous structure have diameters in the range of 1–2 μm. The obtained EDX spectra show that along with iron (Fe), measurable amounts of K, Ca, Mn, Si, and Al were identified (Figure S6). These are typical elemental constituents in the burnt vegetation ashes (Biedermann & Obernberger, 2005; Bodí et al., 2014; Gabet & Bookter, 2011). Using transmission electron microscopy observations, further insights on the morphology of nano-sized particulates in the charred soil material could be gained (Pawluta & Hercman, 2016). Examples of typical clusters of carbon-rich spherules (Figure 2a,c) and characteristic circular structures (Figure 2g,h) give further evidence on the pyrogenic origin of the observed magnetic enhancement.

## 3.4 | Elemental composition of dry vegetation, burnt vegetation residues, and ashes from recent wildfires

Results from XRF analyses of the element concentrations (Appendix B) reveal the dominant presence of Ca, Si, K, and Fe. Other nutrients such as P and S were identified, accounting for less than 4-g/kg dry weight. Plotting the mass-specific magnetic susceptibility of the ashes as a function of their Fe content (Figure 3a) shows that white ashes from high-temperature burning exhibit much stronger magnetic signal as compared with the other ashes of black color and the charred vegetation having similar total Fe content. The elemental content in charred organic matter and ashes shows also typical differentiation related to the type of vegetation—broadleaf, coniferous, and grassland (Figure 3b). Systematically higher Mn and P contents in branches, dry leaves, and charred leaves from hornbeam (*Carpinus putoensis*) at site VL is observed as compared with charred pine bark, needles, and ashes from pine trees (*Pinus nigra*) at the STK site. The white ash sampled under an oak tree (*Quercus pubescens*) at the STK site exhibits higher P content as well. Similarly, the enhanced Mn and P contents

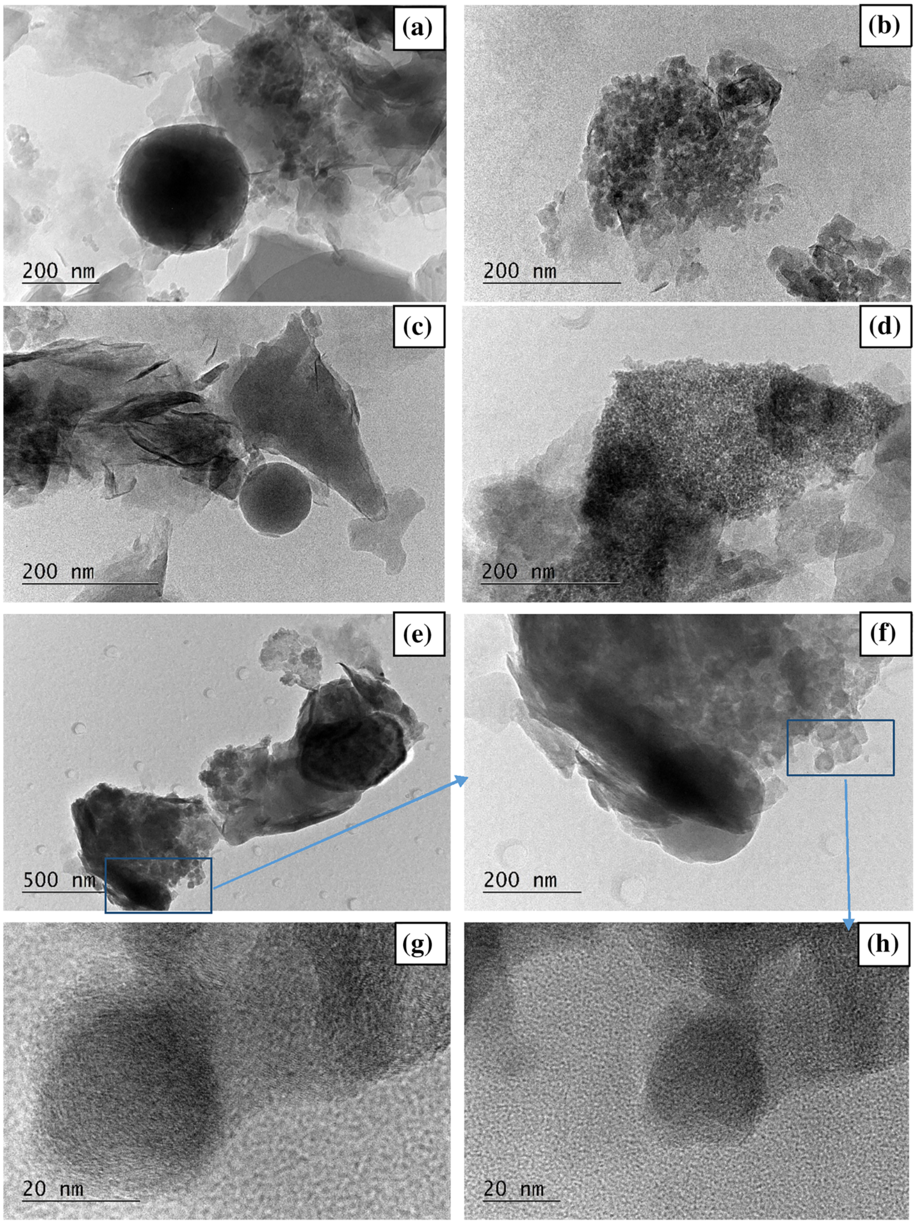


**FIGURE 2** Transmission electron microscope images of pyrogenic materials: (a–c) profile PAN, sample from depth 0–1 cm; (d) profile M, sample from depth 10.5–11 cm with visible charcoal and ash content; (e,f) profile BR, sample from depth 0.5–1 cm; and (g,h) magnified image of typical C-rich particulates, marked by a rectangle in (f) [Colour figure can be viewed at wileyonlinelibrary.com]

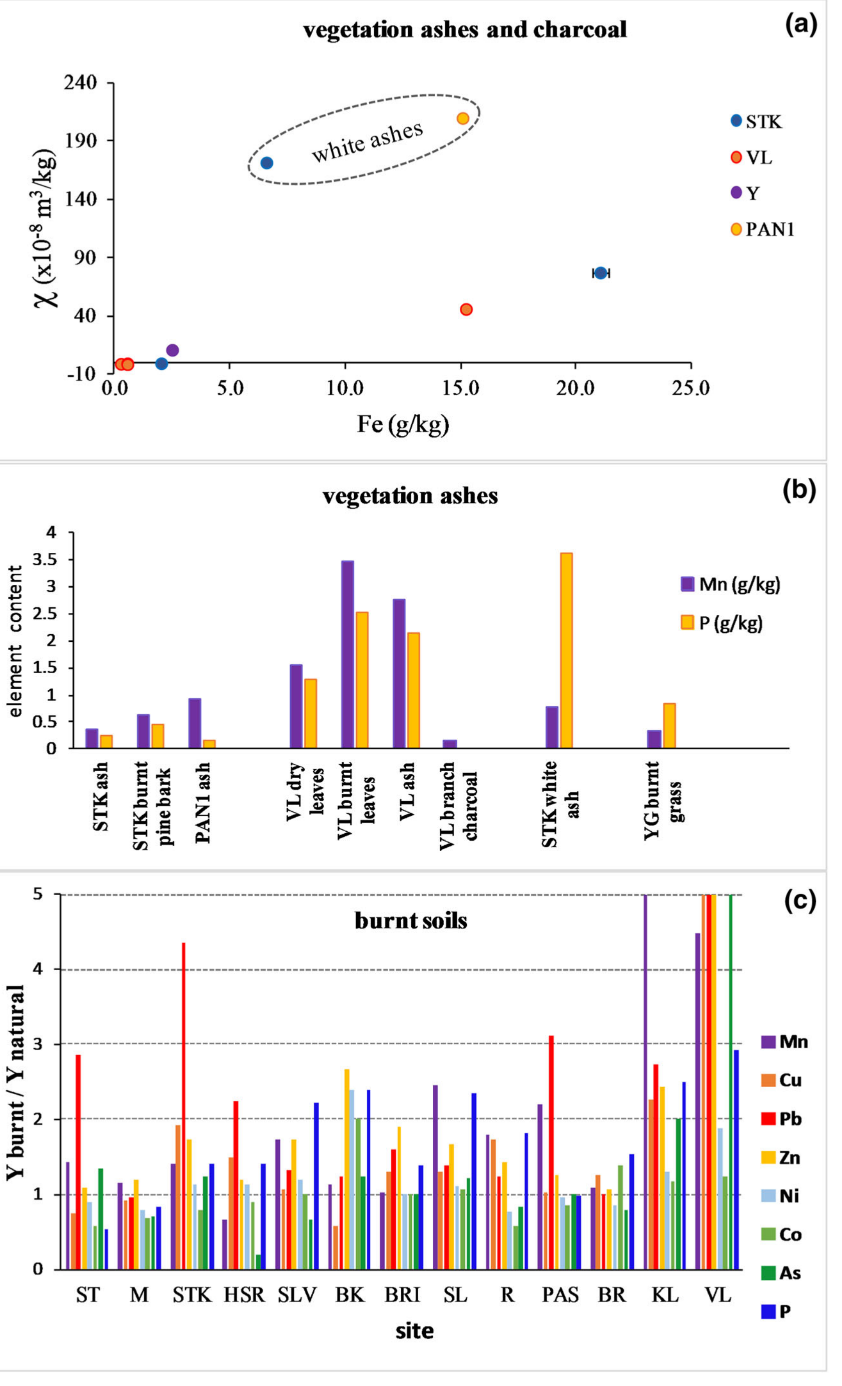


**FIGURE 3** (a) Mass-specific magnetic susceptibility (χ) as a function of Fe content for ashes and charcoal from different wildfire-affected locations; (b) Content of manganese (Mn) and phosphorous (P) in vegetation, ashes, and charcoal from different locations; and (c) normalized by the nonburnt content of chemical elements in fire-affected soil levels [Colour figure can be viewed at wileyonlinelibrary.com]

in burnt soils coming from the vegetation ash additions are found after normalizing the measured elemental concentrations in burnt topsoils to the corresponding content in the natural nonburnt soil profiles (Figure 3c). The observed enrichment with heavy metals (Co, Cu, Pb, Zn, and Ni) in burnt soils (normalized values higher than 1) is another commonly observed phenomenon, reflecting the incorporation of particulates from anthropogenic emissions into the vegetation cover.

Bulk mineralogy identified by powder X-ray diffraction analysis (Figure S7) is represented by quartz, mica, plagioclase, and calcite in the white ashes. Charred vegetation (pine tree bark) revealed no crystalline mineral phases but exhibited only the typical bell-like diffraction curve for the amorphous materials. White ash from the PAN location contains also clinoptilolite (zeolite), montmorillonite, and cristobalite, minerals typical for the volcanic rocks in the area, accommodated in the ash through atmospheric fallout in the forest.

### 3.5 | Pyrogenic magnetic enhancement and changes in nutrients content as a result of wildfires

Plotting the calculated pyrogenic magnetic enhancement as a function of wildfire severity reveals a positive relationship between the two parameters (Figure 4). The dispersal of points within each category (strong—1, moderate—2, and weak—3) is probably related to the effect

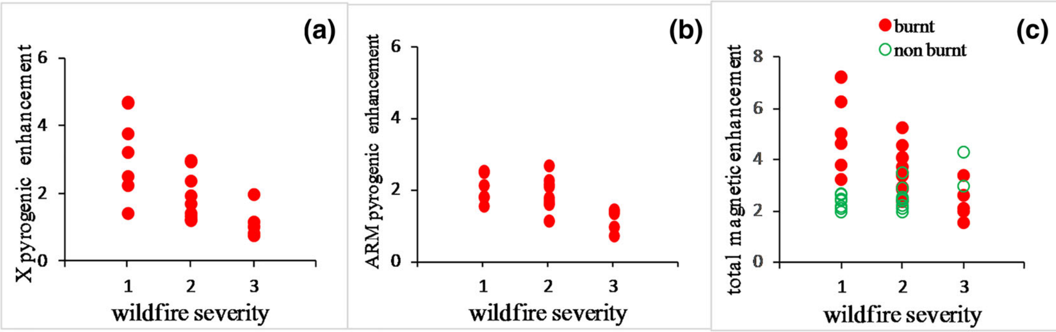


**FIGURE 4** Pyrogenic magnetic enhancement, calculated for the burnt soil levels with the highest magnetic signal: (a) pyrogenic enhancement of magnetic susceptibility as a function of wildfire severity; (b) pyrogenic enhancement of ARM; (c) total pyrogenic magnetic enhancement, calculated as a sum of (a) and (b). Green symbols represent the natural pedogenic magnetic enhancement of nonburnt soil profiles [Colour figure can be viewed at wileyonlinelibrary.com]

of additional factors that play a role for the observed changes after a wildfire such as the type of vegetation, time elapsed since fire, and climate. The first factor is not playing a role for Group 1, as far as all sites suffering strong wildfires were pine forests. However, in Group 2 (moderate wildfires), sites with different vegetation cover were included—pine, oak, mixed conifer, and broadleaf forests (see Table 1). An additional factor could be possible nonaccuracy in assignment of fire severity for wildfires occurred long time ago. In order to check whether the natural pedogenic magnetic enhancement is really taken into account using the chosen normalization approach, we have plotted the corresponding 'pedogenic magnetic enhancement' calculated in a similar way, that is, dividing the enhanced magnetic signal to that one of a deeper level from the parent rock material usually (exceptions are the soil profiles developed on loess under grass vegetation [profiles PLV, RZG, KO] and a Vertisol profile BR). The observed opposite distribution of the values in relation to burnt soil profiles (Figure 4) suggests that the chosen approach is successful. The empirically established relationship between mass-specific magnetic susceptibility of natural soil samples and the content of organic carbon ($C_{org}$) is described by a loglinear regression (Figure 5a). The superimposed plot of burnt soil samples on this relationship reveals similar, although more scattered, distribution shifted towards higher magnetic susceptibility and $C_{org}$ values. Exceptions from this behavior are samples from soils developed on strongly magnetic granitic rocks, whose magnetic signature is governed by the coarse-grained magnetite fraction in the parent material, and as such, an opposite negative relationship between χ and $C_{org}$ is found (Figure 5b). Considering the relative change in $C_{tot}$, calculated as $C_{tot}$ (burnt)/$C_{tot}$ (natural) = $C_{tot\text{-}pyrogenic\ change}$ for the uppermost soil layers, a tendency of greater pyrogenic enhancement for sites under lower wildfire severity is observed (Figure 5c). At the same time, discrimination among plots with different vegetation cover is still maintained. The effect of climate on the development of carbon and nitrogen pools after wildfire is explored through the scatterplot between $C_{org}$/N and the MAP for the respective site (Figure 5d). The ratio $C_{org}$/N for the fire-affected soil levels shows consistent increase with increasing the MAP values for the corresponding locations. The same ratio calculated for the natural nonburnt soil profiles does not follow such dependence (Figure 5d). On the other hand, P content in the burnt soils also shows affinity to the fire intensity (Figure 6a), being systematically lower at sites affected by strong wildfires. This effect is superimposed on the underlying lower P content in ashes from pine trees as compared with broadleaf species, as shown earlier in Figure 3b. The association between combined fire-induced and pedogenic magnetic enhancement carried by strongly magnetic iron oxides and P content is also revealed by plotting the ratio χ/Fe as a function of P (Figure 6b). Normalization of χ by total Fe content represents the share of the total iron involved in strongly magnetic oxide form. As far as strong wildfires lead to high-temperature impact on the vegetation cover and the organic layer, they are accompanied by conversion of organic carbon to the pyrogenic form, which may partly be more recalcitrant (González-Pérez et al., 2004).

## 4 | DISCUSSION

### 4.1 | Pyrogenic magnetic enhancement—Pathways and characterization of mineral phases

Revealing the role, specific characteristics, and properties of pyrogenic magnetic phases in shaping the magnetic recording along soil profiles has been the subject of a number of previous studies (Blake, Wallbrink, Doerr, Shakesby, & Humphreys, 2006; Kletetschka & Banerjee, 1995; Maxbauer, Feinberg, & Fox, 2016b; Oldfield & Crowther, 2007; Roman, Johnson, & Geiss, 2013). The ultimate aim of constructing robust methodology for identification and discrimination of fire-produced iron oxides meets inevitable difficulties related to the superposition of the effects from all environmental as well as intrinsic genetic factors playing a role in the establishment of soil magnetic mineralogy. The results from the present study advance this knowledge by using the data from different wildfire severities, soil types, different vegetation covers, climates, and parent rock lithologies. Mineral magnetic diagnostic experiments revealed that soil samples (burnt and unburnt) as well as vegetation ashes have uniform magnetic mineralogy, dominated by magnetite and/or maghemites with unblocking temperatures in the range between 570 and 640 °C (Figure S3). As far as each of the IRM components (soft, intermediate,

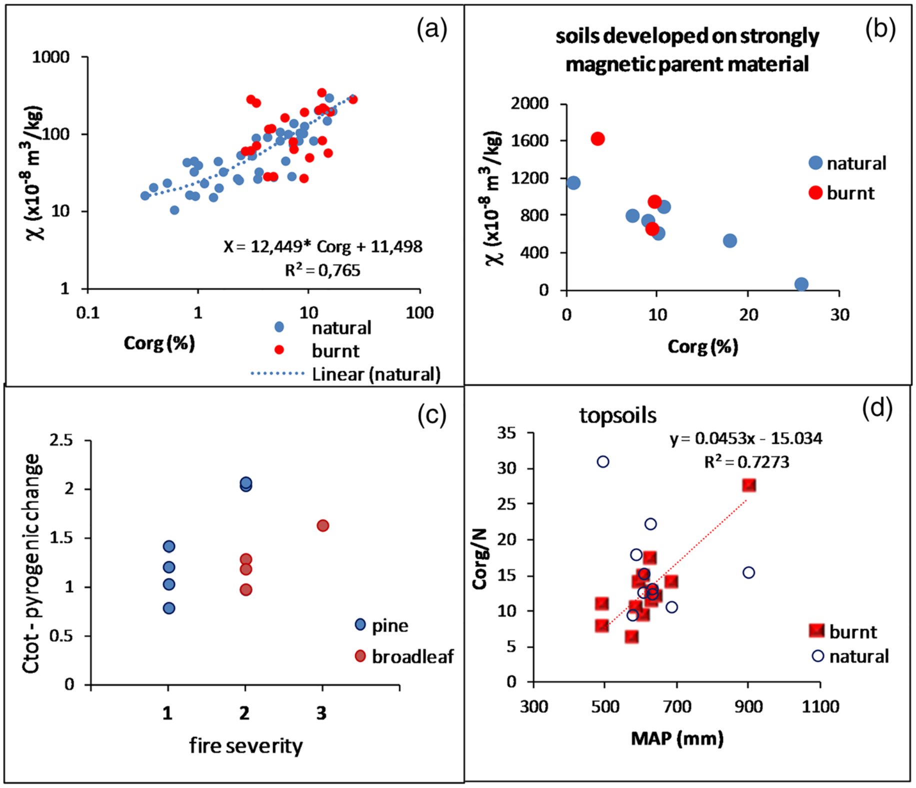


**FIGURE 5** Relationship between organic carbon content ($C_{org}$) and mass-specific magnetic susceptibility (χ) for (a) natural and fire-affected soils developed on weakly to moderately magnetic parent materials and (b) soils developed on strongly magnetic parent igneous rocks (sites VIT and GO from Table 1); (c) pyrogenic change of the total carbon content ($C_{tot\ -\ pyrogenic}$) as a function of wildfire severity; and (d) ratio $C_{org}$/N for the topmost levels as a function of mean annual precipitation (MAP) values of the sampled locations of burnt and natural, not burnt soil profiles [Colour figure can be viewed at wileyonlinelibrary.com]

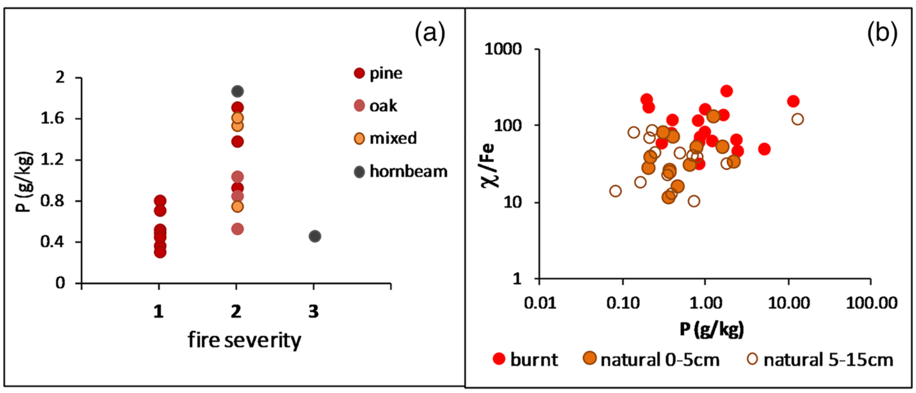


**FIGURE 6** (a) Relationship between fire severity and P content in burnt soils and (b) relationship between the portion of strongly magnetic iron oxides in the burnt soil levels estimated by the ratio χ/Fe and phosphorous content [Colour figure can be viewed at wileyonlinelibrary.com]

and hard) may theoretically include iron oxides of lithogenic, pedogenic, and pyrogenic origin at the same time, the only way of evaluating the amount, contribution, and properties of the pyrogenic fraction is to compare burnt and natural soils with vegetation ashes. The observed similarities in the major unblocking temperatures and demagnetization behavior of samples coming from one site and representing different materials (burnt, natural, and ashes) strongly supports the working hypothesis that magnetic mineralogy of pyrogenic origin is very much similar to the pedogenic minerals widely identified in soils—magnetite, maghemite, and hematite (Jordanova, 2016; Maher, 1986; Maxbauer et al., 2016b). The concave unblocking spectra of the low-coercivity components of the composite IRM (Figure S3) suggest that the grain size distribution of the pyrogenic magnetite fraction spans a wide range. The latter is clearly reflected in the permanently observed significant pyrogenic enhancement of the burnt soils not only of magnetic susceptibility, which is governed by the presence of nanosized SP particles ($d$ < 0.03 μm), but also of larger stable single-domain grains ($d$ ~ 0.03 – 0.05 μm; Dunlop, 1973), contributing to the ARM signal (Figures 1 and S2). The coercivity of the dominating soft component, isolated from IRM acquisition curves decomposition (Figure S4) varies between 34 and 40 mT and thus corresponds to magnetite/maghemite (e.g., Dunlop & Özdemir, 1997). On the basis of the obtained higher coercivity of this soft component in burned soils (Figure S4) as compared with nonburned material, it could be assumed that the grain size of magnetically soft minerals, appeared as a result of fire, is finer. This conclusion is in agreement with the major findings on fire-altered soils (Oldfield & Crowther, 2007). The high-coercivity component is present in all samples (both burnt and nonburnt), and it thus can be assigned to a lithogenic/pedogenic hematite or goethite (Maxbauer et al., 2016a).

A closer look at the contribution of the two components of the defined pyrogenic magnetic enhancement—χ and ARM (Figure 4)—reveals that higher discrimination power between wildfires of different severity is provided by the value of magnetic susceptibility, whereas ARM among the three categories (strong, moderate, and weak) shows less variability. Consequently, we may argue that strong wildfires lead to the formation of higher amounts of strongly magnetic SP particles and lower amounts of stable single-domain grains. Moderate- and weak-severity wildfires produce less SP fraction but similar to the severe-fires amount of single-domain magnetite (maghemite). A low degree of pyrogenic magnetic enhancement for sites with grass vegetation that experienced weak wildfires is consistent with the results, reported by Roman et al. (2013), who studied magnetic properties of burnt by prescribed fires loessic soils in Iowa (USA). Further characterization of the pyrogenic magnetic fraction is obtained through scanning electron microscopy/transmission electron microscopy observations (Figures 2, S5, and S6). Coarser spherical Fe-containing particles in the charred wood (Figure S5a) and burnt soil material (Figure S5b–f) show close association with the organic residues and most probably originated from the wildfire emissions as a result of combustion of vegetation cover (Chakrabarty et al., 2006). High intensity peaks of Fe in the obtained EDX spectra (Figure S6) further confirm their dominant contribution to the total magnetic signal of the burnt soils. Smaller, nanometer-sized spherules observed in the burnt soils under pine forest (Figure 2) resemble well the configuration and morphology reported for pyrogenic organic matter (Preston & Schmidt, 2006). Strongly magnetic properties of the vegetation ash, especially of white ashes, are testified by the observed relationship between their total Fe content and magnetic susceptibility shown in Figure 3a. Similar high values of magnetic susceptibility of ashes from wood and grass combustion, cigarette burning, and so on, are well documented in a number of studies (Jordanova et al., 2006; Lu et al., 2000; McClean & Kean, 1993). Along with the observed enrichment of the burnt soils with strongly magnetic iron oxides from vegetation ashes, the latter brings important changes in the element and nutrients contents as well (Figure 3b,c). As revealed by the XRF analysis of ashes (Appendix B and Figure 3b), they contribute to the net gain in the burnt soil phosphorous and manganese contents to different degrees depending on the type of vegetation (broadleaf, needleleaf, and grasses). Similarly to other studies on chemical composition of wood ash and other biofuels (Gabet & Bookter, 2011; Knapp & Insam, 2011; Misra, Ragland, & Baker, 1993) major constituents are Ca, K, Al, Si, P, S, Fe, and Mn (Appendix B). The overall enhancement of the total P content in burnt soils as compared with their unburnt counterparts (estimated by the ratio $P_{burnt}/P_{natural} > 1$) is observed in most of the sites studied, similar to the results reported by other authors (Harden, Mack, Veldhuis, & Gower, 2003; Kelly, Montgomery, & Reid, 2018; Santín, Otero, Doerr, & Chafer, 2018). Exceptions are sites M and ST, for which an effective depletion is obtained. These two sites, however, are characterized by low pH values (see Table 1), which may play a role for secondary translocation of heavy metals along soil depth (Alloway, 1995). Enhanced content of heavy metals (Cu, Pb, Zn, Ni, Co, and As) in burnt soils is most pronounced for Pb and Zn (Figure 3c), which is consistent with other reports (Campos, Abrantes, Keizer, Vale, & Pereira, 2016). Because most of the sites are located in mountain areas and often hardly assessable, the presence of nearby pollution sources could be excluded. This supports the assumption that increased content of heavy metals is due to long-range transport of pollutants trapped in the tree canopy and deposited as ash after wildfire.

### 4.2 | Stability of pyrogenic magnetic enhancement of soils over time and statistical significance of the link between magnetic enhancement of burnt soils and wildfire severity

An important question widely discussed in the studies devoted to wildfire effects on soil properties is the time dependence of the observed changes. The effect of the 'time elapsed since fire' factor is difficult to explore because of superposition of various confounding factors. Considering the group of sites with pine forests only, a weak tendency for diluting enhancement with time passed could be assumed (Appendix C). The latter experimental evidence suggests that the amount of strongly magnetic minerals in the burnt soils, at least partly, is due to the minerals originating from the burnt vegetation ashes. This observation is in line with the suggested contribution of the strongly magnetic fraction from the vegetation ash to the total pyrogenic magnetic enhancement of burnt soils (e.g., Jordanova, 2017; Jordanova et al., 2018). On the other hand, no consistent relationship between only pyrogenic magnetic susceptibility and time since fire is observed. The obtained trend of decreasing pyrogenic magnetic enhancement with increasing time passed since a fire event (Appendix C) obviously depends on the wildfire severity, so a similar pyrogenic magnetic enhancement could be estimated for various fire severities depending on the time passed since the event. This decreasing pyrogenic magnetic signal could be well explained by the occurrence of low-temperature oxidation (Dunlop & Özdemir, 1997) of the strongly magnetic pyrogenic minerals. The latter may be directly produced in fire emissions at high temperatures and subsequently deposited on the surface (Heilman, Liu, Urbanski, Kovalev, & Mickler, 2014). Yet another possible explanation for the presence of high-temperature originating spherules is their transport from anthropogenic pollution sources (Yan, Sun, Weiss, Liang, & Chen, 2015). However, in our case, their systematic presence in fire-affected topsoils (Figures 2 and S5) testifies wildfire as the most probable origin. An additional pathway of formation of strongly magnetic particles as a result of wildfire occurrence is the postfire microbially mediated magnetite synthesis, intensified due to the effect of explosive growth of heterotrophic bacteria in response to increased nutrients availability (Mataix-Solera et al., 2009). Recently published research on the time evolution of the magnetic susceptibility of burnt soil from an experimental fire also supports this hypothesis (Jordanova et al., 2019).

In order to check the statistical significance of the relationship obtained between magnetic enhancement of burnt soils and wildfire severity (Figure 4), we have performed ANOVA one-way analysis of variance of the data. Plot of mean values of variables ($\chi_b/\chi_n$, $ARM_b/ARM_n$, and $\chi_b/\chi_n + ARM_b/ARM_n$) for each group of sites characterized by the corresponding fire severity with the 95% confidence intervals, and the results from the Tukey honestly significant difference post hoc test are shown in Appendix D. It can be seen that differences between total magnetic enhancement ($\chi_b/\chi_n + ARM_b/ARM_n$) of strong (1) and weak (3) wildfires are the most significant. Furthermore, wildfires of severity 1 and 2 also produce significantly different magnetic enhancement, presented by $\chi_b/\chi_n$ and $\chi_b/\chi_n + ARM_b/ARM_n$ (Appendix D), whereas $ARM_b/ARM_n$ is statistically different for fire severity 1 and 3 only.

### 4.3 | Changes in magnetic properties and nutrients content in soils as a result of wildfires

As pointed out by Wiesmeier et al. (2019), Fe and Al oxides are good indicators for soil organic carbon (SOC) storage from microscale to landscape scale. Using the magnetic characteristics of soils, especially magnetic susceptibility, as an indicator for SOC content overwhelms the problem of costly, time-consuming, and laborious soil fractionation analyses for determination of the content of Fe and Al oxides by classical chemical extractions. The obtained experimental results from our study reveal the presence of loglinear dependence between magnetic susceptibility ($\chi$) and the organic carbon content $C_{org}$ (Figure 5a). This relationship is better retained by samples from natural soils from the uppermost (0.5- to 2-cm depth) layers as well as from deeper (15–20 cm) depth intervals. Taking into account the fact that the present experimental data are coming from different soil profiles developed at different landscapes, climate, and parent material influences, the obtained correlation strongly warrants the applicability of magnetic susceptibility as a suitable "functional characteristic" for soil's SOC content (Vogel et al., 2018). Similar results on a local scale have been reported for natural Haplic Chernozems from south Moravia (Czech Republic) by Jakšık et al. (2016) and Calcisols from Spain (Quijano, Chaparro, Marié, Gaspar, & Navas, 2014). The negative trend, observed for the forest soils, developed on strongly magnetic parent material (granite; Figure 5b), reflects the dominance of the lithogenic magnetic fraction in the soil magnetic properties and the increasing concentration of strongly magnetic coarse magnetite grains with depth. Scattered data corresponding to burnt soil samples in Figure 5a suggest that fire exerts complex effects on the nutrients pool, which is reflected not only in the $C_{org}$ content and properties but rather in its relative change to N pool. This synergetic response to fire is seen in Figure 5d, showing the relationship between MAP at different sites and the ratio $C_{org}/N$. In contrast to nonburnt sites, $C_{org}/N$ for the topmost levels of the burnt soils systematically increases with increasing MAP. It suggests that postfire recovery of the organic carbon and nitrogen pools is more sensitive to the climate conditions. In particular, MAP values are known to strongly affect microbial activities (Wang, Wang, Han, & Deng, 2018; Zhou & Wang, 2015). On the other hand, there could be an additional interaction between SOC stock and the fresh additions of pyrogenic carbon and nitrogen from the combusted organic matter, as shown by Bradford, Fierer, and Reynolds (2008). The authors report an increased SOC formation with increased additions of inorganic nitrogen in the soil system. Another commonly observed phenomenon is a decrease of $C_{tot}$ content in ashes and mineral soil with increased fire severity (Adkins, Sanderman, & Miesel, 2019; Araya, Fogel, & Berhe, 2017; Pereira, Úbeda, & Martín, 2012). Such a trend is found also in the present study, revealed by the pyrogenic change after wildfire and separated according to the type of vegetation cover—needleleaf or broadleaf forests (Figure 5c).

Changes in the content of carbon, nitrogen, and other important nutrients in soils influence vegetation growth and soil fertility, being important ecological aspects of fire-affected landscapes (Alcañiz, Outeiro, Francos, & Úbeda, 2018; Santín et al., 2018; Santín & Doerr, 2016; Sawyer, Bradstock, Bedward, & Morrison, 2018). The response of P content to the effects of wildfires is further revealed in our data (Figure 6a). Due to the increasing temperatures reached during severe wildfire events, P is partly volatilized or entirely escapes the soil system when temperature reaches 500 °C or higher (Bodí et al., 2014). Similar to the relationship between $C_{org}$ and magnetic susceptibility in Figure 5a, total P content shows an increase with increasing the normalized by total Fe content magnetic susceptibility (Figure 6b). The normalization by total Fe implies that P is intimately bounded to the strongly magnetic pedogenic and pyrogenic Fe oxides, and most of it is probably present as organic fraction. Similar experimental linear relationships between magnetic susceptibility and total P content are reported for various soil profiles (Chernozems, Luvisols, Planosols, Alisols, Fluvisols) from Bulgaria, which being not normalized to total Fe content, form different regression lines depending on the parent material and its lithogenic magnetic signal (Jordanova, 2017).

## 5 | CONCLUSIONS

Wildfire-affected soils show systematic enrichment of the topmost 0–2 cm with strongly magnetic iron oxides magnetite and/or maghemite. They are formed during wildfire from the fire emissions and vegetation ashes or shortly post fire due to intensified microbially mediated production of nanomagnetite. The latter process is partly triggered by the amount of local annual precipitation. The strongly magnetic particles found in burnt soils are characterized by spherical shape, typical sizes between 0.100 and 1–2 μm. They are found in close association with the charred organic matter and vegetation residues. The observed degree of pyrogenic magnetic enhancement of fire-affected soils is strongly related to the wildfire severity. The highest pyrogenic magnetic enhancement is linked to the occurrence of strong wildfires in pine forests and is dominated by superparamagnetic (SP) fraction. Wildfires of lower severity cause lower pyrogenic enhancement with larger relative contribution of single-domain ferrimagnetic grains. The magnetic signal of wildfire-affected soils can be used successfully for estimation of the changes in the total carbon content as a result of fire, as well as spatial variability of fire severity and the pyrogenic change in nutrients content, especially N and P.

## ACKNOWLEDGMENTS

This work was financially supported by the Bulgarian National Science Fund through the project DFNI K02/13 and the INTERREG-POCTEP: "Centro Ibérico para la Investigación y Lucha contra Incendios Forestales" (0753_CILIFO_5_E) project. We also thank the Servicio Central de Apoyo a la Investigación (SCAI) of the University of Córdoba for technical support.

## CONFLICT OF INTEREST

Authors declare no conflict of interest.

## ORCID

*Neli Jordanova* https://orcid.org/0000-0002-9959-4456

## REFERENCES

Adkins, J., Sanderman, J., & Miesel, J. (2019). Soil carbon pools and fluxes vary across a burn severity gradient three years after wildfire in Sierra Nevada mixed-conifer forest. *Geoderma*, *333*, 10–22. https://doi.org/10.1016/j.geoderma.2018.07.009

Alcañiz, M., Outeiro, L., Francos, M., & Úbeda, X. (2018). Effects of prescribed fires on soil properties: A review. *Science of the Total Environment*, *613–614*, 944–957. https://doi.org/10.1016/j.scitotenv.2017.09.144

Alloway, B. J. (1995). *Heavy metals in soil* (2nd ed.). London: Blackie Academic and Professional, Chapman and Hall.

Araya, S. N., Fogel, M. L., & Berhe, A. A. (2017). Thermal alteration of soil organic matter properties: A systematic study to infer response of Sierra Nevada climosequence soils to forest fires. *The Soil*, *3*, 31–44. https://doi.org/10.5194/soil-3-31-2017

Barrón, V., & Torrent, J. (2013). Iron, manganese and aluminium oxides and oxyhydroxides. In F. Nieto, & K. J. T. Livi (Eds.), *Minerals at the nanoscale*. *European Mineralogical Union Volume 14 – Chapter 9*. London: Mineralogical Society of Great Britain & Ireland. https://doi.org/10.1180/EMU-notes.14.9

Bento-Gonçalves, A., Vieira, A., Úbeda, X., & Martín, D. (2012). Fire and soils: Key concepts and recent advances. *Geoderma*, *191*, 3–13. https://doi.org/10.1016/j.geoderma.2012.01.004

Biedermann, F., & Obernberger, I. (2005). Ash-related problems during biomass combustion and possibilities for a sustainable ash utilisation. *Proceedings of the International Conference. "World Renewable Energy Congress" (WREC)*, Oxford: Elsevier, 120–124.

Blake, W. H., Wallbrink, P. J., Doerr, S. H., Shakesby, R. A., & Humphreys, G. S. (2006). Magnetic enhancement in wildfire-affected soil and its potential for sediment-source ascription. *Earth Surface Processes and Landforms*, *31*, 249–264. https://doi.org/10.1002/esp.1247

Bodí, M. B., Martin, D. A., Balfour, V. N., Santín, C., Doerr, S. H., Pereira, P., … Mataix-Solera, J. (2014). Wildland fire ash: Production, composition and eco-hydro-geomorphic effects. *Earth-Science Reviews*, *130*, 103–127. https://doi.org/10.1016/j.earscirev.2013.12.007

Bradford, M. A., Fierer, N., & Reynolds, J. F. (2008). Soil carbon stocks in experimental mesocosms are dependent on the rate of labile carbon, nitrogen and phosphorus inputs to soils. *Functional Ecology*, *22*, 964–974. https://doi.org/10.1111/j.1365-2435.2008.01404.x

Campos, I., Abrantes, N., Keizer, J. J., Vale, C., & Pereira, P. (2016). Major and trace elements in soils and ashes of eucalypt and pine forest plantations in Portugal following a wildfire. *Science of the Total Environment*, *572*, 1363–1376. https://doi.org/10.1016/j.scitotenv.2016.01.190

Carrancho, A., & Villalaín, J. J. (2011). Different mechanisms of magnetisation recorded in experimental fires: Archaeomagnetic implications. *Earth and Planetary Science Letters*, *312*, 176–187. https://doi.org/10.1016/j.epsl.2011.10.006

Certini, G. (2014). Fire as a soil-forming factor. *Ambio*, *43*, 191–195. https://doi.org/10.1007/s13280-013-0418-2

Chakrabarty, R. K., Moosmuller, H., Garro, M. A., Arnott, W. P., Walker, J., Susott, R. A., … Hao, W. M. (2006). Emissions from the laboratory combustion of wildland fuels: Particle morphology and size. *Journal of Geophysical Research*, *111*, D07204. https://doi.org/10.1029/2005JD006659

Cornell, R., & Schwertmann, U. (2003). *The iron oxides. Structure, properties, reactions, occurrence and uses*. Weinheim, New York: Wiley-VCH.

Dunlop, D., & Özdemir, O. (1997). In D. Edwards (Ed.), *Rock magnetism. Fundamentals and frontiers*. *Cambridge Studies in Magnetism*. New York: Cambridge University Press.

Dunlop, D. J. (1973). Superparamagnetic and single-domain threshold sizes in magnetite. *Journal of Geophysical Research*, *78*, 1780–1793. https://doi.org/10.1029/JB078i011p01780

Evans, M. E., & Heller, F. (2003). *Environmental magnetism: Principles and applications of enviromagnetics*. *International Geophysics Series*. (p. 299). Paris: Academic Press.

Gabet, E., & Bookter, A. (2011). Physical, chemical and hydrological properties of Ponderosa pine ash. *International Journal of Wildland Fire*, *20*, 443–452. https://doi.org/10.1071/WF09105

Goforth, B., Graham, R., Hubbert, K., Zanner, C., & Minnich, W. (2005). Spatial distribution and properties of ash and thermally altered soils after high-severity forest fire, southern California. *International Journal of Wildland Fire*, *14*, 343–354. https://doi.org/10.1071/WF05038

González-Pérez, J., González-Vila, F., Almendros, G., & Knicker, H. (2004). The effect of fire on soil organic matter—A review. *Environment International*, *30*, 855–870. https://doi.org/10.1016/j.envint.2004.02.003

Harden, J. W., Mack, M., Veldhuis, H., & Gower, S. T. (2003). Fire dynamics and implications for nitrogen cycling in boreal forests. *Journal of Geophysical Research: Atmospheres*, *108*(D3), WFX-4. https://doi.org/10.1029/2001JD000494

Heilman, W. E., Liu, Y., Urbanski, S., Kovalev, V., & Mickler, R. (2014). Wildland fire emissions, carbon, and climate: Plume rise, atmospheric transport, and chemistry processes. *Forest Ecology and Management*, *317*, 70–79. https://doi.org/10.1016/j.foreco.2013.02.001

Jakšik, O., Kodesová, R., Kapicka, A., Klement, A., Fér, M., & Nikodem, A. (2016). Using magnetic susceptibility mapping for assessing soil degradation due to water erosion. *Soil and Water Research*, *11*, 105–113. https://doi.org/10.17221/233/2015-SWR

Jiang, Z., Liu, Q., Roberts, A. P., Barrón, V., Torrent, J., & Zhang, Q. (2018). A new model for transformation of ferrihydrite to hematite in soils and sediments. *Geology*, *46*, 987–990. https://doi.org/10.1130/G45386.1

Jordanova, D., Jordanova, N., Barrón, V., & Petrov, P. (2018). The signs of past wildfires encoded in the magnetic properties of forest soils. *Catena*, *171*, 265–279. https://doi.org/10.1016/j.catena.2018.07.030

Jordanova, N. (2016). *Soil magnetism. Applications in pedology, environmental science and agriculture* (p. 446). Amsterdam: Academic Press, Elsevier.

Jordanova, N. (2017). Applications of soil magnetism. In *Soil magnetism. Applications in pedology, environmental science and agriculture* (pp. 395–436). XXX: Academic Press, Elsevier. DOI: 10.1016/B978-0-12-809239-2.00010-3

Jordanova, N., Jordanova, D., Henry, B., Le Goff, M., Dimov, D., & Tsacheva, T. (2006). Magnetism of cigarette ashes. *Journal of Magnetism and Magnetic Materials*, *301*, 50–66. https://doi.org/10.1016/j.jmmm.2005.06.008

Jordanova, N., Jordanova, D., Mokreva, A., Ishlyamski, D., & Georgieva, B. (2019). Temporal changes in magnetic signal of burnt soils—A compelling three years pilot study. *Science of the Total Environment*, *669*, 729–738. https://doi.org/10.1016/j.scitotenv.2019.03.173

Keeley, J. E. (2009). Fire intensity, fire severity and burn severity: A brief review and suggested usage. *International Journal of Wildland Fire*, *18*, 116–126. https://doi.org/10.1071/WF07049

Kelly, R. W., Montgomery, I., & Reid, N. (2018). Differences in soil chemistry remain following wildfires on temperate heath and blanket bog sites of conservation concern. *Geoderma*, *315*, 20–26. https://doi.org/10.1016/j.geoderma.2017.11.016

King, J., Banerjee, S., Marvin, J., & Ozdemir, O. (1982). A comparison of different magnetic methods for determining the relative grain size of magnetite in natural materials: Some results from lake sediments. *Earth and Planetary Science Letters*, *59*, 404–419. https://doi.org/10.1016/0012-821X(82)90142-X

Kletetschka, G., & Banerjee, S. K. (1995). Magnetic stratigraphy of Chinese loess as a record of natural fires. *Geophysical Research Letters*, *22*, 1341–1343. https://doi.org/10.1029/95GL01324

Knapp, B. A., & Insam, H. (2011). Recycling of biomass ashes: Current technologies and future research needs. In H. Insam, & B. A. Knapp (Eds.), *Recycling of biomass ashes* (pp. 1–16). Berlin: Springer. https://doi.org/10.1007/978-3-642-19354-5_1

Knicker, H. (2007). How does fire affect the nature and stability of soil organic nitrogen and carbon? A review. *Biogeochemistry*, *85*, 91–118. https://doi.org/10.1007/s10533-007-9104-4

Kruiver, P., Dekkers, M., & Heslop, D. (2001). Quantification of magnetic coercivity components by the analysis of acquisition curves of isothermal remanent magnetisation. *Earth and Planetary Science Letters*, *189*, 269–276. https://doi.org/10.1016/S0012-821X(01)00367-3

Le Borgne, E. (1955). Abnormal magnetic susceptibility of the top soil. *Annales de Geophysique*, *11*, 399–419.

Lowrie, W. (1990). Identification of ferromagnetic minerals in a rock by coercivity and unblocking temperature properties. *Geophysical Research Letters*, *17*, 159–162. https://doi.org/10.1029/GL017i002p00159

Lu, H., Liu, T., Gu, Z., Liu, B., Zhou, L., Han, J., & Wu, N. (2000). Effect of burning C3 and C4 plants on the magnetic susceptibility signal in soils. *Geophysical Research Letters*, *27*, 2013–2016. https://doi.org/10.1029/2000GL011459

Maher, B. A. (1986). Characterisation of soils by mineral magnetic measurements. *Physics of the Earth and Planetary Interiors*, *42*, 76–92. https://doi.org/10.1016/S0031-9201(86)80010-3

Maher, B. A. (1988). Magnetic properties of some synthetic sub-micron magnetites. *Geophysical Journal International*, *94*, 83–96. https://doi.org/10.1111/j.1365-246X.1988.tb03429.x

Maher, B. A. (2016). Palaeoclimatic records of the loess/palaeosol sequences of the Chinese Loess Plateau. *Quaternary Science Reviews*, *154*, 23–84. https://doi.org/10.1016/j.quascirev.2016.08.004

Mataix-Solera, J., Cerdá, A., Arcenegui, V., Jordán, A., & Zavala, L. M. (2011). Fire effects on soil aggregation: A review. *Earth-Science Reviews*, *109*, 44–60. https://doi.org/10.1016/j.earscirev.2011.08.002

Mataix-Solera, J., Guerrero, C., García-Orenes, F., Bárcenas, G. M., & Torres, M. P. (2009). Forest fire effects on soil microbiology. In M. J. Haigh (Ed.), *Land Reconstruction and Management Series. Vol. 5: Fire effects on soils and restoration strategies*. Volume Editors: A. Cerdà and P. R. Robichaud. Oxford, UK: CRC Press, Oxford Brookes University.

Maxbauer, D., Feinberg, J., & Fox, D. (2016a). MAX UnMix: A web application for unmixing magnetic coercivity distributions. *Computers & Geosciences*, *95*, 140–145. https://doi.org/10.1016/j.cageo.2016.07.009

Maxbauer, D. P., Feinberg, J. M., & Fox, D. L. (2016b). Magnetic mineral assemblages in soils and paleosols as the basis for paleoprecipitation proxies: A review of magnetic methods and challenges. *Earth-Science Reviews*, *155*, 28–48. https://doi.org/10.1016/j.earscirev.2016.01.014

McClean, R. G., & Kean, W. F. (1993). Contributions of wood ash magnetism to archaeomagnetic properties of fire pits and hearths. *Earth and Planetary Science Letters*, *119*, 387–394. https://doi.org/10.1016/0012-821X(93)90146-Z

Melton, E. D., Swanner, E. D., Behrens, S., Schmidt, C., & Kappler, A. (2014). The interplay of microbially mediated and abiotic reactions in the biogeochemical Fe cycle. *Nature Reviews Microbiology*, *12*, 797–808. https://doi.org/10.1038/nrmicro3347

Misra, M. K., Ragland, K. W., & Baker, A. J. (1993). Wood ash composition as a function of furnace temperature. *Biomass and Bioenergy*, *4*, 103–116. https://doi.org/10.1016/0961-9534(93)90032-Y

Oldfield, F., & Crowther, J. (2007). Establishing fire incidence in temperate soils using magnetic measurements. *Palaeogeography, Palaeoclimatology, Palaeoecology*, *249*, 362–369. https://doi.org/10.1016/j.palaeo.2007.02.007

Panayotov, M., Gogushev, G., Tsavkov, E., Vasileva, P., Tsvetanov, N., Kulakowski, D., & Bebi, P. (2017). Abiotic disturbances in Bulgarian mountain coniferous forests—An overview. *Forest Ecology and Management*, *388*, 13–28. https://doi.org/10.1016/j.foreco.2016.10.034

Pawluta, M., & Hercman, H. (2016). Transmission electron microscopy (TEM) as a tool for identification of combustion products: Application to black layers in speleothems. *Annales Societatis Geologorum Poloniae*, *86*, 237–248. https://doi.org/10.14241/asgp.2016.004

Pereira, P., Úbeda, X., & Martín, D. A. (2012). Fire severity effects on ash chemical composition and water-extractable elements. *Geoderma*, *191*, 105–114. https://doi.org/10.1016/j.geoderma.2012.02.005

Preston, C. M., & Schmidt, M. W. I. (2006). Black (pyrogenic) carbon: A synthesis of current knowledge and uncertainties with special consideration of boreal regions. *Biogeosciences*, *3*, 397–420. https://doi.org/10.5194/bg-3-397-2006

Quijano, L., Chaparro, M. A. E., Marié, D. C., Gaspar, L., & Navas, A. (2014). Relevant magnetic and soil parameters as potential indicators of soil conservation status of Mediterranean agroecosystems. *Geophysical Journal International*, *198*, 1805–1817. https://doi.org/10.1093/gji/ggu239

Robertson, D. J., & France, D. E. (1994). Discrimination of remanence-carrying minerals in mixtures, using isothermal remanent magnetisation acquisition curves. *Physics of the Earth and Planetary Interiors*, *84*, 223–234. https://doi.org/10.1016/0031-9201(94)90074-4

Roman, S. A., Johnson, W. C., & Geiss, C. E. (2013). Grass fires—An unlikely process to explain the magnetic properties of prairie soils. *Geophysical Journal International*, *195*, 1566–1575. https://doi.org/10.1093/gji/ggt349

Rummery, T. A., Bloemendal, J., Dearing, J., & Oldfield, F. (1979). The persistence of fire-induced magnetic oxides in soils and lake sediments. *Annales de Geophysique*, *35*, 103–107.

Santín, C., & Doerr, S. H. (2016). Fire effects on soils: The human dimension. *Philosophical Transactions of the Royal Society, B: Biological Sciences*, *371*, 20150171. https://doi.org/10.1098/rstb.2015.0171

Santín, C., Otero, X. L., Doerr, S., & Chafer, C. (2018). Impact of a moderate/high-severity prescribed eucalypt forest fire on soil phosphorous stocks and partitioning. *Science of the Total Environment*, *621*, 1103–1114. https://doi.org/10.1016/j.scitotenv.2017.10.116

Sawyer, R., Bradstock, R., Bedward, M., & Morrison, R. J. (2018). Fire intensity drives post-fire temporal pattern of soil carbon accumulation in Australian fire-prone forests. *Science of the Total Environment*, *610–611*, 1113–1124. https://doi.org/10.1016/j.scitotenv.2017.08.165

Schwertmann, U. (1988). Occurrence and formation of iron oxides in various pedoenvironments. In J. Stucki, B. Goodman, & U. Schwertmann (Eds.), *Iron in soils and clay minerals* (Vol. 217). *NATO ASI Series, Series C: Mathematical and Physical Sciences*. (pp. 267–308). Boston: Reidel Publ. Company.

Stockhausen, H. (1998). Some new aspects for the modelling of isothermal remanent magnetisation acquisition curves by cumulative log Gaussian functions. *Geophysical Research Letters*, *25*, 2217–2220. https://doi.org/10.1029/98GL01580

Vogel, H.-J., Bartke, S., Daedlow, K., Helming, K., Kögel-Knabner, I., Lang, B., … Wollschläger, U. (2018). A systemic approach for modeling soil functions. *The Soil*, *4*, 83–92. https://doi.org/10.5194/soil-4-83-2018

Walden, J., Oldfield, F., & Smith, J. (Eds.) (1999). *Environmental magnetism. A practical guide*. *Technical Guide No 6*. (p. 239). London: Quaternary Research Association.

Wang, S., Wang, X., Han, X., & Deng, Y. (2018). Higher precipitation strengthens the microbial interactions in semi-arid grassland soils. *Global Ecology and Biogeography*, *27*, 570–580. https://doi.org/10.1111/geb.12718

Wiesmeier, M., Urbanski, L., Hobley, E., Lang, B., von Lützowa, M., Marin-Spiottad, E., … Kögel-Knabner, I. (2019). Soil organic carbon storage as a key function of soils—A review of drivers and indicators at various scales. *Geoderma*, *333*, 149–162. https://doi.org/10.1016/j.geoderma.2018.07.026

Yan, Y., Sun, Y. B., Weiss, D., Liang, L. J., & Chen, H. Y. (2015). Polluted dust derived from long-range transport as a major end member of urban aerosols and its implication of non-point pollution in northern China. *Science of the Total Environment*, *506-507*, 538–545. https://doi.org/10.1016/j.scitotenv.2014.11.071

Zhou, Z. H., & Wang, C. K. (2015). Reviews and syntheses: Soil resources and climate jointly drive variations in microbial biomass carbon and nitrogen in China's forest ecosystems. *Biogeosciences*, *12*, 6751–6760. https://doi.org/10.5194/bg-12-6751-2015

## SUPPORTING INFORMATION

Additional supporting information may be found online in the Supporting Information section at the end of the article.

**How to cite this article:** Jordanova N, Jordanova D, Barrón V. Wildfire severity: Environmental effects revealed by soil magnetic properties. *Land Degrad Dev*. 2019;30:2226–2242. https://doi.org/10.1002/ldr.3411

## APPENDIX A


**FIGURE A1** Photographs of representative profiles of soils affected by wildfires [Colour figure can be viewed at wileyonlinelibrary.com]

## APPENDIX B

**TABLE B1** Magnetic susceptibility (χ) and mean value of elements content (g/kg) with the corresponding SD for vegetation, ashes, and charcoal samples

| Name | X × $10^{-8}$ $m^3$/kg | Al (g/kg) | SD-Al | Si (g/kg) | SD-Si | P (g/kg) | SD-P | S (g/kg) | SD-S | K (g/kg) | SD-K | Ca (g/kg) | SD-Ca | Ti (g/kg) | SD-Ti | Mn (g/kg) | SD-Mn | Fe (g/kg) | SD-Fe | Cu (g/kg) | SD-Cu | Zn (g/kg) | SD-Zn |
|---|---|---|---|---|---|---|---|---|---|---|---|---|---|---|---|---|---|---|---|---|---|---|---|
| STK ash | 77.33 | 16.754 | 0.443 | 74.994 | 2.258 | 0.248 | 0.051 | 1.897 | 0.924 | 11.022 | 0.936 | 8.390 | 0.510 | 3.902 | 0.239 | 0.376 | 0.008 | 21.037 | 0.340 | 0.042 | 0.005 | 0.080 | 0.004 |
| STK burnt pine bark | −0.55 | 2.086 | 0.120 | n.d. | 0.000 | 0.448 | 0.057 | 0.453 | 0.000 | n.d. | 0.000 | 68.000 | 1.467 | 0.285 | 0.057 | 0.626 | 0.015 | 2.015 | 0.016 | 0.047 | 0.004 | 0.054 | 0.001 |
| PAN1 ash | 209.69 | 9.294 | 0.436 | 71.408 | 2.403 | 0.174 | 0.020 | n.d. | 0.000 | 7.972 | 0.217 | 8.377 | 0.229 | 2.011 | 0.027 | 0.927 | 0.028 | 15.071 | 0.254 | 0.379 | 0.007 | 2.639 | 0.072 |
| VL dry leaves | −0.58 | 0.961 | 0.210 | 4.820 | 1.668 | 1.282 | 0.124 | 1.246 | 0.818 | 15.280 | 0.808 | 27.743 | 1.907 | 0.261 | 0.010 | 1.560 | 0.108 | 0.547 | 0.013 | 0.026 | 0.002 | 0.029 | 0.003 |
| VL burnt leaves | −1.01 | 0.990 | 0.003 | n.d. | 0.000 | 2.515 | 0.148 | 1.588 | 0.912 | 20.164 | 1.140 | 35.513 | 1.155 | 0.211 | 0.025 | 3.462 | 0.086 | 0.268 | 0.023 | 0.035 | 0.003 | 0.046 | 0.001 |
| VL ash | 46.05 | 6.714 | 0.525 | 46.894 | 2.123 | 2.135 | 0.232 | 2.175 | 0.611 | 8.274 | 0.108 | 95.257 | 5.011 | 2.214 | 0.225 | 2.761 | 0.401 | 15.216 | 0.680 | 0.072 | 0.004 | 0.101 | 0.007 |
| VL branch charcoal | −1.39 | 1.010 | 0.167 | n.d. | | n.d. | | n.d. | | 0.205 | | 9.491 | 0.564 | n.d. | | 0.165 | 0.025 | 0.549 | 0.067 | 0.032 | 0.002 | 0.011 | 0.001 |
| STK white ash | 171.47 | 5.544 | 0.478 | n.d. | | 3.615 | 0.098 | 5.271 | 0.427 | 20.583 | 0.426 | 284.127 | 6.281 | 0.855 | 0.073 | 0.793 | 0.061 | 6.572 | 0.093 | 0.235 | 0.004 | 1.021 | 0.026 |

Abbreviations: n.d., not determined; SD, standard deviation.

## APPENDIX C

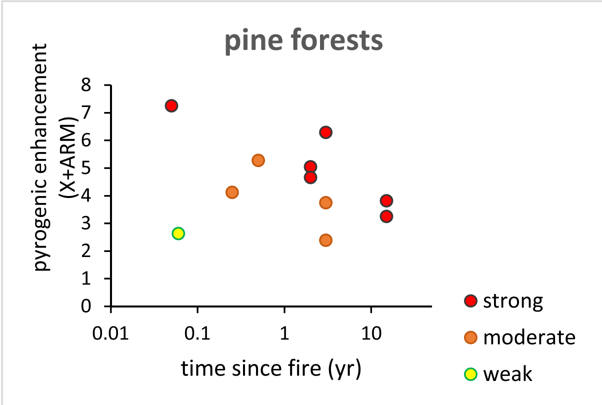


**FIGURE C1** Pyrogenic magnetic enhancement (χ + ARM) as a function of time past since fire (only sites with pine vegetation are included) [Colour figure can be viewed at wileyonlinelibrary.com]

## APPENDIX D

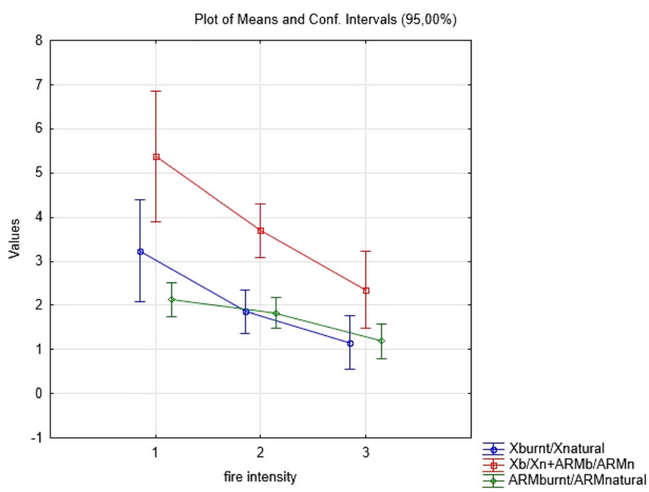


**FIGURE D1** Mean values of the pyrogenic enhancement of magnetic susceptibility, ARM, and total enhancement with their corresponding standard deviations for strong, moderate, and weak wildfires [Colour figure can be viewed at wileyonlinelibrary.com]

The table below summarizes the results from ANOVA one-way analysis of variance test for significance.

**TABLE D1** Tukey (honestly significant difference) test with unequal number (*N*) observations

| | Variable | | | | | | | | |
|---|---|---|---|---|---|---|---|---|---|
| | $\chi_b/\chi_n$ | | | $ARM_b/ARM_n$ | | | $\chi_b/\chi_n + ARM_b/ARM_n$ | | |
| | Fire intensity | | | | | | | | |
| | 1 | 2 | 3 | 1 | 2 | 3 | 1 | 2 | 3 |
| | Mean value of variable | | | | | | | | |
| Group | 3.236 | 1.865 | 1.160 | 2.129 | 1.829 | 1.188 | 5.365 | 3.693 | 2.349 |
| 1 | | ***0.0225*** | ***0.0038*** | | 0.416 | ***0.0076*** | | ***0.0309*** | ***0.0014*** |
| 2 | ***0.0225*** | | 0.4286 | 0.4157 | | 0.075 | ***0.0309*** | | 0.1695 |
| 3 | ***0.0038*** | 0.428 | | ***0.0076*** | 0.075 | | ***0.0014*** | 0.1695 | |

*Note*. Marked differences between groups are significant at $p < .05$.